J. Fluid Mech. (1981), *vol.* 103, *pp.* 479–504
Printed in Great Britain

Mean-flow measurements in the three-dimensional boundary layer over a body of revolution at incidence

By B. R. RAMAPRIAN, V. C. PATEL AND D. H. CHOI

Iowa Institute of Hydraulic Research,
The University of Iowa, Iowa 52242

(Received 22 January 1979 and in revised form 21 April 1980)

An experimental study of the three-dimensional turbulent boundary layer on a body of revolution is reported. The data correspond to axisymmetric flow as well as the flow at an angle of incidence of 15°, and include surface pressure distributions and the distribution of the magnitude and orientation of the velocity vector in the boundary layer. The results clearly exhibit most of the complexities encountered in practical three-dimensional boundary-layer flows, such as viscid–inviscid interaction, reversal of cross-flow, open separation and onset of longitudinal vortices. Major implications of these results on the development of computation procedures are discussed.

1. Introduction

The study reported here was undertaken in order to elucidate several important features of three-dimensional turbulent boundary-layer flow. A body of revolution at incidence was chosen, instead of more simple configurations, not only because it is representative of shapes of aero- and hydrodynamic interest, but also because the boundary layer over it exhibits several fundamental flow phenomena that are poorly understood at the present time.

Three-dimensional turbulent boundary-layer data are required for the development and calibration of prediction procedures as well as for the assessment of their limitations. A review of the existing data has been made recently by Johnston (1976). Of the nearly eighty sets of so-called three-dimensional turbulent boundary-layer measurements examined there, many are restricted to flows whose properties are invariant in one space direction, a majority do not document the most important parameters in sufficient detail, and a very few consider the flow in the neighbourhood of truly three-dimensional separations. The present experiment was designed to provide a detailed set of mean-flow data and specifically to explore the conditions leading to the reversal of the cross-flow and occurrence of a non-singular separation that is often followed by the roll-up of the boundary layer to form longitudinal vortices. The earlier work of Maskell (1955) and the calculations of Wang (1972, 1974*a*, *b*, *c*, 1975) and others have established some general features of three-dimensional flow separation. These have been confirmed in some detail by the recent flow-visualization studies of Han & Patel (1977, 1979) in laminar flow. The latter formed a prelude to the present study in which attention is focused on the measurement of the pressure and mean-velocity distributions in a turbulent flow. Since the flow on a body of revolution at incidence is accompanied by significant viscous–inviscid flow interaction, the data also shed some light on the implications of such interactions relative to the development of successful

0022-1120/81/4616-3370 $02.00

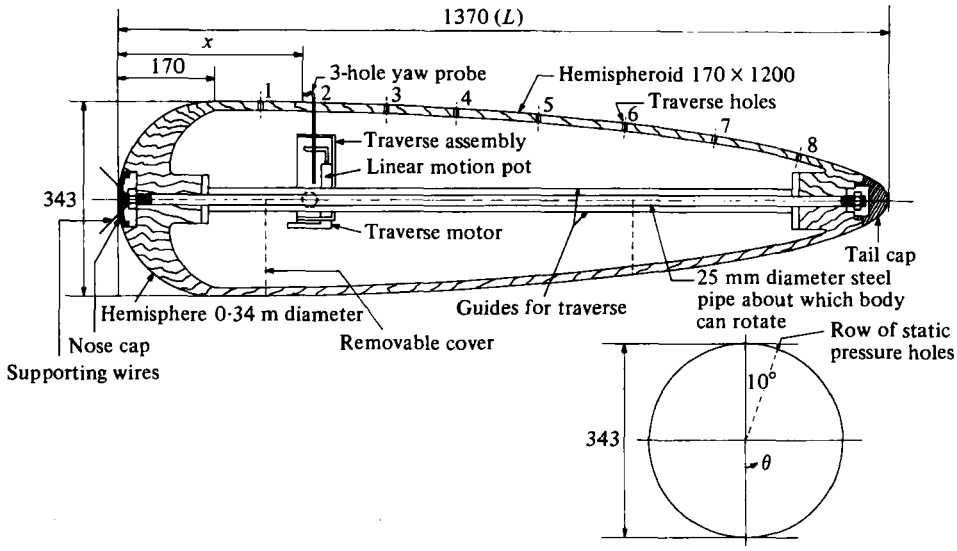

FIGURE 1. Constructional details of the model (all dimensions are in mm).

Station	1	2	3	4	5	6	6	8
x/L	0·176	0·241	0·333	0·426	0·537	0·648	0·759	0·870

solution procedures. It is not at all certain that the usual thin three-dimensional boundary-layer calculation procedures can adequately handle reversing cross-flows, open separations and attendant interactions, although their success or failure in practical applications would depend largely on the manner in which these flow features are treated. While turbulence modelling is also an important factor, the results of the present study indicate that proper treatment of the flow features noted above may play a far greater role in determining the overall success of prediction procedures.

Surface pressure distributions and profiles of the two primary components of mean velocity have been measured on a body of revolution at an angle of attack of 15°. These measurements have been used to infer the magnitude and approximate direction of the wall shear-stress vector. Measurements have also been made in the axisymmetric (zero incidence) configuration to provide a useful reference.

2. Experimental programme

2.1. *Design and construction of the body*

The selection of a suitable shape for the test body was an important first step in the present study. Several alternatives were considered in a preliminary investigation which involved flow visualization on scaled models in a hydraulic flume and a wind tunnel (see Han & Patel 1977) as well as potential-flow and boundary-layer calculations. The geometry shown in figure 1 was finally selected. The flow-visualization studies indicated that, at Reynolds numbers (based on body length) greater than about 4×10^5, there was no singular separation (i.e. axial flow reversal) anywhere on this body upto an incidence, α, of 30°. It was also found that at moderate angles of incidence ($\alpha \sim 20°$) the flow was quite steady over 95 % of the body length in spite

of the existence of a vortical flow (circumferential flow reversal) on the leeward side. The boundary-layer calculations indicated that thicknesses ranging from 6 to 40 mm may be obtained at a Reynolds number of about 10^6. The preliminary studies thus led to the conclusion that reliable boundary-layer data could be obtained in the range $0{\cdot}2 < x/L < 0{\cdot}8$, where x is the axial distance measured from the nose and L is the body length.

The dimensions and construction of the model are shown in figure 1. The shape combines a hemispherical nose with a hemispheroidal rear. The model is hollow and was made of treated and seasoned pine-wood laminations. This form of construction, along with surface treatment consisting of six coats of enamel paint covered by a top layer of acrylic paint, was used to prevent moisture absorption and consequent warping. The exterior surface of the body had a glossy finish. The body was machined in one piece, except for the two end caps, and a removable lid was cut out to gain access to the interior. The weight of the body was supported by the axial 25 mm outside diameter stainless-steel tube. The nose and tail caps were rigidly fixed to this tube. The body was suspended in the wind tunnel by means of wires attached to the cap at each end. The tube and the caps supported at the two ends therefore formed the fixed part of the model. The hollow wooden body could be rotated about the steel tube and clamped by friction clamps to the latter at any circumferential position. This position could be read on the angular scale provided on the nose cap. The lid, used to gain easy access to the interior of the body, was located on the side diametrically opposite the location of the pressure taps and probe holes. A 12 mm diameter hole in the tail cap allowed the pressure tubing and electrical connections to be brought out of the body.

The traversing assembly was mounted inside the model and could be fixed in any longitudinal position in the range $0{\cdot}15 < x/L < 0{\cdot}7$. The mechanism could also be swivelled about an axis perpendicular to the longitudinal axis and clamped in position. This enabled the line of traverse to be aligned with the normal to the body surface at all longitudinal positions. The traverse was activated by a small d.c. motor. The probe displacement was measured by a linear-motion potentiometer to an accuracy of $\pm 0{\cdot}05$ mm. The locations of the traverse stations are shown in the legend of figure 1.

Further details on the preliminary studies leading to the selection of the body shape and the construction of the model are given in Ramaprian, Patel & Choi (1978).

2.2. *Instrumentation*

The wall static pressure was measured using a row of forty-eight wall taps. These were 1 mm diameter holes and were spaced sufficiently close to obtain a reliable measurement of the longitudinal pressure gradient. In order to reduce mutual interference between the static pressure holes and the 3 mm diameter probe holes, the two sets of holes were located along lines separated by 10°. In addition to the set of longitudinal pressure taps, circumferential rows of wall pressure taps at 45° intervals were provided at three longitudinal locations along the body. These were useful in aligning the body in the tunnel as well as checking whether the body rotated about its axis without any wobble. All the pressure traps were connected to a rotary scanivalve mounted on the inside wall of the body. The 48-position scanivalve was controlled from outside the wind tunnel and could be used to connect any one of the pressure holes to the pressure transducer/manometer system. Some of the preliminary measurements were made

using a micromanometer, but the bulk of the measurements were made using a pressure transducer. The pressure transducer output was electronically averaged over a period of 10 seconds.

The total head distributions in the boundary layer in the plane of symmetry were measured using a conventional total-head tube of outside diameter 0·62 mm. The total head was read using a pressure transducer and the associated averaging electronics mentioned earlier. The velocity in the boundary layer was obtained using these data along with the *corresponding* wall static pressure (i.e. the wall static pressure at the same axial and circumferential position as the probe location). No correction was applied for any variation of static pressure normal to the surface. The accuracy in pressure measurement is estimated to be 0·05 mm of water. Velocity measurements are expected to be accurate to within 0·5 %.

For boundary-layer measurements at points other than those on the plane of symmetry, a three-hole yaw probe was used. This was constructed from three 0·8 mm outer diameter hypodermic tubes soldered together side by side. The outer two tubes were chamfered at 45°. The pressure outputs from the three tubes, with the probe aligned with the body generator, were measured using pressure transducers, and used to determine the magnitude and direction of the velocity vector from the yaw-probe calibration curves obtained in a two-dimensional channel (air) flow.

Let P_1, P_2, P_3 be the pressures measured by the tubes 1, 2 and 3, respectively, P_s, $\mathbf{Q}$ be the local static pressure and flow velocity vector, respectively, and γ be the angle between the velocity vector and the probe axis. We can then define the following calibration coefficients:

$$K_{is} = (P_i - P_s)/\tfrac{1}{2}\rho Q^2 = f_i(\gamma, R) \quad (i = 1, 2, 3)$$

and

$$K = -(P_1 - P_2)/(P_2 - P_3) = f_4(\gamma, R),$$

where R is a Reynolds number based on some characteristic dimension of the probe and the magnitude, Q, of the velocity vector. Preliminary calibrations performed at velocities 6, 12 and 20 m s^{-1} showed that the effect of probe Reynolds number was negligible at velocities larger than 12 m s^{-1}. The final calibration curves were therefore obtained at only a single reference velocity of about 22 m s^{-1} and extended over the range $-45° < \gamma < 45°$. Details of the calibration procedure and the use of the calibration curves to determine Q and γ are given in Ramaprian, Patel & Choi (1978). The estimated accuracy of the measurements with the yaw probe is ± 1 % for Q and $\pm 1°$ for γ.

The wall shear stress, τ_w, in axisymmetric flow was determined by using the total-head probe itself as a Preston tube and the calibration of Patel (1965). This technique was also employed along the plane of symmetry with the body at incidence, thus assuming that the influence of flow convergence or divergence on the law of the wall is negligible. In the case of the general three-dimensional boundary layer, the three readings of the yaw probe touching the surface were used to determine the magnitude and direction of τ_w through a special calibration obtained from two-dimensional channel flow. In the calibration experiments, the probe was mounted so as to be just touching the wall (like a Preston tube) and the pressure readings $(P_1 - P_s)_w$, $(P_2 - P_s)_w$ and $(P_3 - P_s)_w$ were recorded at several yaw angles. Also, a reference total-head tube

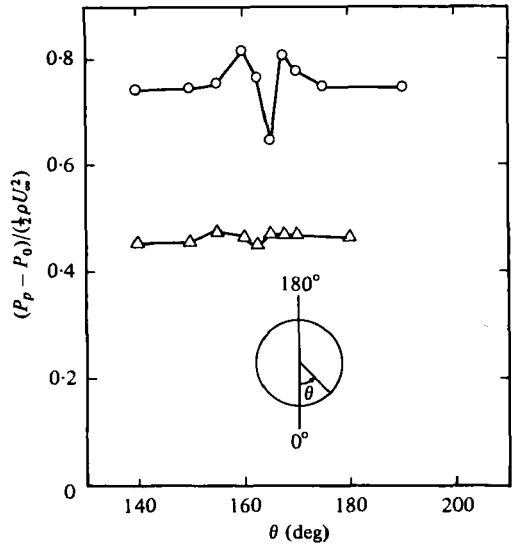

FIGURE 2. Results of the circumferential surveys for assessing the effect of wire wakes in axisymmetric flow. Survey behind one wire only is shown. ○, station 1 (x/L = 0·176); △, station 3 (x/L = 0·333).

was used as a conventional Preston tube and its reading $(P_p - P_s)$ was measured. These led to the calibration coefficients

$$K_{isw} = \frac{(P_i - P_s)_w}{(P_p - P_s)} \quad \text{for} \quad i = 1, 2, 3, \quad K_w = -\frac{(P_1 - P_2)_w}{(P_2 - P_3)_w},$$

which are expected to depend, in general, upon the probe Reynolds number, the angle between the wall shear stress and the probe axis (γ_w), and the local rate of skew $\partial\gamma/\partial y$ of the mean velocity profile (which is zero in the channel flow but large in the inner region of the three-dimensional boundary layer being studied). The influence of Reynolds number could be neglected on the basis of the previous observation, but that of the rate of skew could not be determined from the calibrations performed in the two-dimensional flow. While using the yaw-probe for measuring the wall shear stress vector in the three-dimensional boundary layer, the angle γ_w was first obtained from the calibration function K_w. This value of γ_w was then used, along with one of the remaining three K functions, to obtain $(P_p - P_s)$. The value so obtained represents an 'equivalent two-dimensional Preston tube reading' in the three-dimensional boundary layer. This reading was used to obtain the magnitude of γ_w from the Preston tube calibration of Patel (1965). It is estimated that (with the choice of the appropriate K function) this procedure yields the magnitude, τ_w, to within 5 % (see Ramaprian *et al.* 1978). There is, however, a considerable uncertainty in the determination of the angle γ_w due to the possible influence of $\partial\gamma/\partial y$ very near the wall. Errors in γ_w as large as 6° may result from this effect (see Johnston 1976).

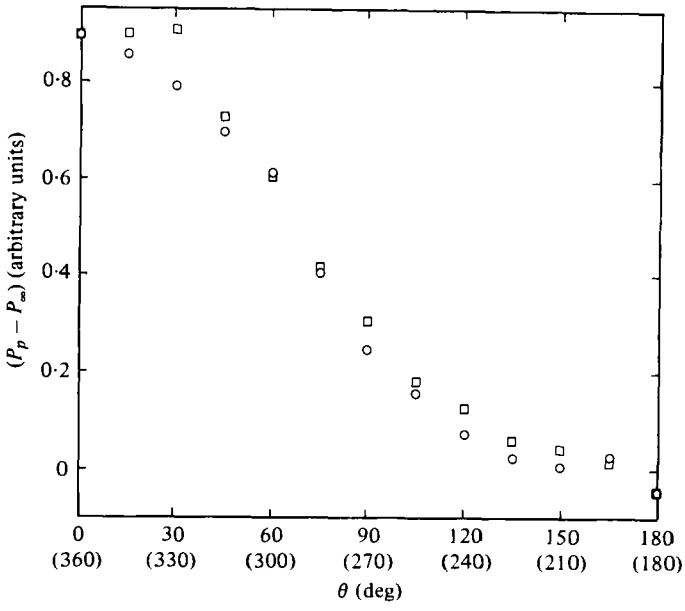

FIGURE 3. Distribution of Preston tube head around the body at station 1. ○, θ = 0–180°; □, θ = 180–360°.

2.3. *Initial tests*

The model was suspended in the 1·67 m octagonal working-section wind tunnel of the Institute by four 14-gauge stainless-steel wires attached to the nose cap and four 10-gauge wires of the same material attached to the tail cap. A 0·76 mm diameter trip wire wrapped around the body and glued to the surface at an axial distance of 56 mm (x/L = 0·04) from the nose, served to promote and fix transition under all experimental conditions.

A detailed study of the effect of the support wires on the downstream flow was made. The effect of the wires on the wall static pressure was found to be negligible even at the first traverse location, station 1. However, there was a perceptible effect of the wires on the wall shear stress particularly at station 1. Several methods were tried, such as use of thinner support wires, varying the angle of slant of the wires, etc., to remove this disturbance. While these resulted in some improvement, the wire wake effect could not be completely eliminated. This effect is seen from figure 2 (corresponding to axisymmetric flow) where typical circumferential variations of the reading, P_p of a Preston tube behind one of the wires are shown at two axial stations. It is seen that the influence of the support wire is confined to a narrow wake region (of a spread of about 20°) behind each wire. Comparison between the results at the two stations also show that this effect is smeared out rapidly in the downstream direction. The boundary-layer traverse locations in the case of the axisymmetric-flow measurements as well as in the plane-of-symmetry measurements at the 15° incidence did not fall in this region and therefore are not affected by the wire wakes. Figure 3 shows the results of a circumferential survey of Preston tube reading at station 1 with the body at 15° incidence. It is seen that, while the distribution does show some indication of the presence of wire wakes (e.g. at θ = 330°), the fairly

smooth distribution suggests that the wire effects have been attenuated significantly. It appears as though the three-dimensional flow quickly smears the individual wakes. The effects of the support-wire wakes will therefore be assumed to be unimportant in all the experiments reported in the present study.

2.4. *Axisymmetric boundary-layer measurements*

The experiments at zero incidence, as well as the angle of incidence experiments performed later, were carried out at a nominal wind-tunnel velocity of 22·0 m s^{-1}. The Reynolds number (based on the length of the body), with this tunnel speed, was $2{\cdot}0 \times 10^6$. The actual reference free-stream velocity U_∞ and free-stream static pressure P_∞ were measured using a standard Prandtl probe (and micromanometer) at a section downstream of the wind tunnel contraction exit and 1·7 m upstream of the nose of the test body. It was ascertained that there was no upstream effect of the body on the flow at this location. The wall static pressure (P_0) distribution was measured along several generators, outside the influence of the wakes of the support wires. Total head traverses were made across the boundary layer at stations 1–6 along the generator $\theta = 0°$. In addition, traverses were made at $\theta = 90$, 180 and 270° at two stations, 2 and 6, in order to check the axial symmetry of the flow. In each of these experiments, the first reading of the total-head tube (with the tube just touching the wall) was used to determine the wall shear stress.

2.5. *Boundary-layer measurements with the body at an angle of incidence*

These measurements were made with the body mounted at a geometric incidence, α, of 15°. This angle was chosen after several exploratory tests were made at other angles. These tests indicated that, at $\alpha = 15°$, the flow would exhibit, to a measurable degree, the various flow phenomena enumerated earlier, and that the flow conditions would still not become so severe as to cause any serious difficulty in measurement using the present instrumentation.

Before beginning the actual measurements, the lateral symmetry of the flow was checked. This was done by recording the circumferential distribution of the reading $(P_t - P_\infty)$ of a total-head tube touching the wall and directed along the generator. While this reading is not a direct measure of the wall shear stress (except for $\theta = 0$ and 180°) it is, nevertheless, a sensitive indicator of lateral symmetry of the flow. The results of this survey are shown in figure 3 which has already been referred to earlier. It can be seen that the data for 0–180° overlap on those for 180–360°. (The apparent departures at a few isolated angular positions are due to the effect of support-wire wakes, as has been noted above.) In view of the lateral symmetry, detailed boundary-layer data were obtained only over one half of the circumference (with the exception of the wall static pressure distribution for $\theta = 270°$).

Surface pressure distribution, in the longitudinal direction, was measured from $\theta = 0$ to $\theta = 180°$ at intervals of 20°. The boundary-layer velocity profiles were measured in two stages. First, velocity profiles were measured in the plane of symmetry, i.e. along $\theta = 0$ and $\theta = 180°$. Since, in this plane, there is no cross-flow, velocity measurements were made using the total-head tube. The profiles were obtained at stations 1–7. Next, the velocity profiles over the remainder of the body surface were measured using the calibrated three-hole yaw probe. Again, as in the case of the total head tube, the effect of any variation of static pressure across the boundary layer was

not considered. It may be mentioned, however, that it is possible to obtain, in principle, the values of P_s (the local static pressure), Q and γ from the three readings of the yaw probe. This may be done by first determining γ in the usual manner, then Q from a calibration curve of $(K_{1s}-K_{2s})$ *vs.* γ, and finally the local P_s from the calibration curve of (say) K_{1s} *vs.* γ. The results of such a procedure indicated that the variation of static pressure across the boundary layer was negligible even at station 6 and $\theta = 150°$, where it may be suspected to be large due to the rapid growth of the boundary layer. It was estimated that the error in Q due to the assumption of constant pressure across the boundary layer was no greater than 1 % even in the worst case.

The yaw probe (with the limitations already mentioned) was also used to determine the wall shear stress at each measuring station.

3. Description of results

In the interest of brevity, only typical results are presented and discussed here. The complete set of data have been tabulated and are available in Ramaprian *et al.* (1978). The tables also provide, where relevant, the values of the various integral parameters.

3.1. *Axisymmetric boundary-layer measurements*

Figure 4 shows the longitudinal pressure distribution at two circumferential positions, namely $\theta = 0$ and 120°. The pressure coefficient, C_p, is defined by

$$C_p = \frac{P_0 - P_\infty}{\frac{1}{2}\rho U_\infty^2},$$

where P_0 is the pressure on the surface, P_∞ and U_∞ are the pressure and velocity in the undisturbed freestream and ρ is the density. The measured distribution of C_p is compared with the inviscid distribution obtained with the method of Landweber & Macagno (1969). The excellent agreement confirms the existence of axial symmetry and indicates that any blockage effect introduced by the presence of the body in the tunnel is negligible.

The velocity distributions across the boundary layer at the first six longitudinal stations along $\theta = 0$ ($x/L = 0{\cdot}176, 0{\cdot}241, 0{\cdot}333, 0{\cdot}426, 0{\cdot}537, 0{\cdot}648$) are shown in figure 5. The velocity profiles measured along $\theta = 180°$ at two of the stations are also shown to indicate the extent of the axial symmetry achieved in the experiment. The velocity profile shape at station 1 is seen to be typical of boundary layers in flows with adverse pressure gradients. Reference to figure 4 shows that the pressure gradient at station 1 is adverse but relaxing. Over most of the flow along the body, the pressure gradient is very mildly adverse. We have, therefore, a case of an axisymmetric turbulent boundary layer relaxing from a strong adverse pressure gradient to near-zero pressure gradient. These data would therefore provide a critical test case for the calibration of a three-dimensional boundary-layer prediction procedure. Historically, the relaxing flow has been one of the more difficult flows to predict, even in two-dimensional situations. The axisymmetric flow involves the additional influence of flow divergence or convergence. The effect of this is seen very clearly from figure 6 which shows the distributions of the integral parameters, namely the momentum thickness Reynolds

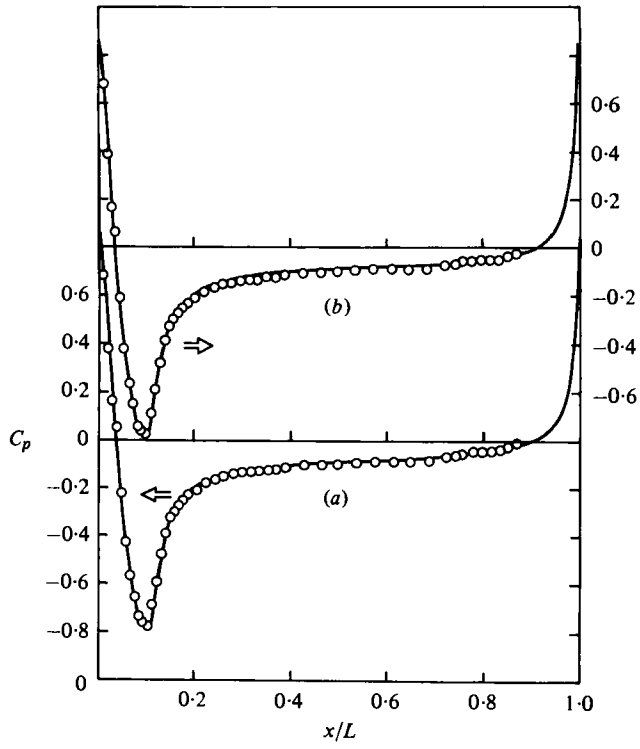

FIGURE 4. Longitudinal distribution of wall static pressure in axisymmetric flow ($\alpha = 0$). (*a*) $\theta = 0°$, (*b*) $\theta = 120°$. ——, inviscid theory; ○, experiment.

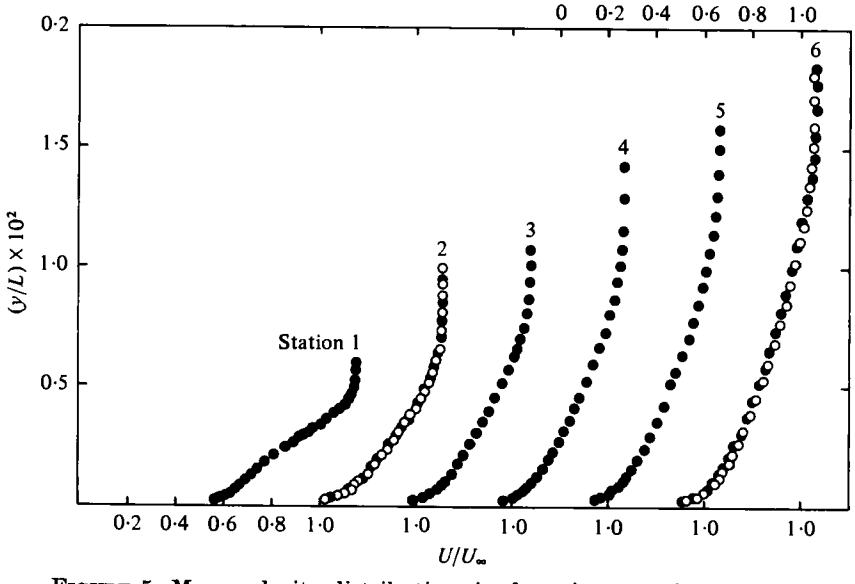

FIGURE 5. Mean velocity distributions in the axisymmetric boundary layer at stations 1 to 6. ●, $\theta = 0°$; θ, ○ $= 180°$.

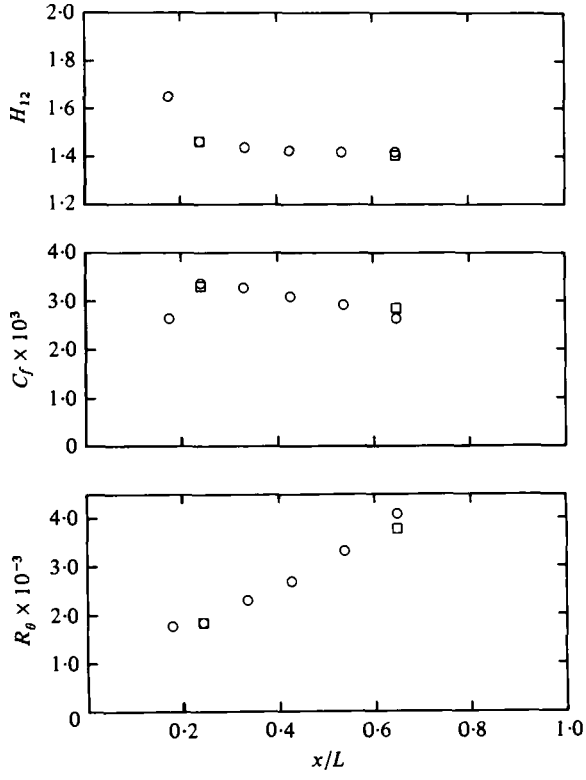

FIGURE 6. Development of the axisymmetric boundary layer along the body. ○, $\theta = 0°$; □, $\theta = 180°$.

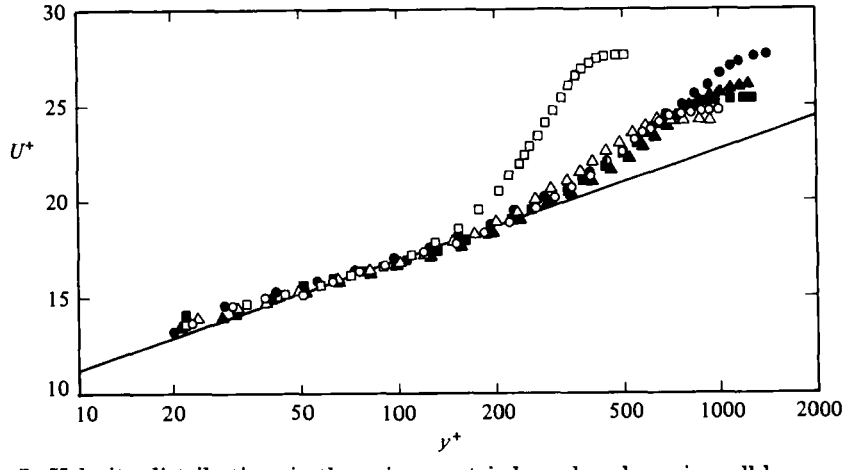

FIGURE 7. Velocity distributions in the axisymmetric boundary layer in wall-layer co-ordinates at the first six stations: □, 1; △, 2; ○, 3; ■, 4; ▲, 5; ●, 6; ——, universal 'log law' ($U^+ = 5{\cdot}75 \log y^+ + 5{\cdot}5$).

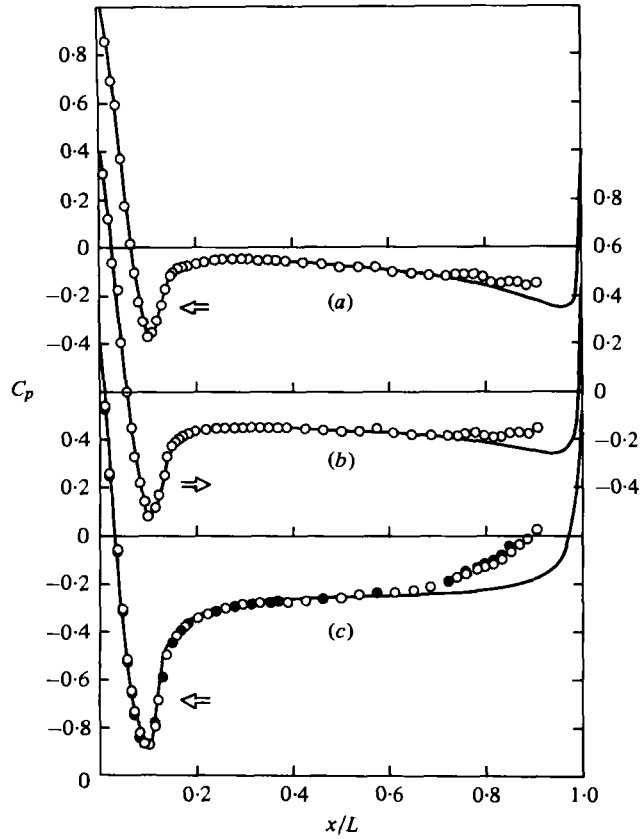

FIGURE 8. Typical longitudinal distributions of wall static pressure on the body of revolution at an angle of incidence of 15°. (*a*) $\theta = 0°$, (*b*) $\theta = 40°$, (c) $\theta = 90°$ (○), 270° (●), (*d*) $\theta = 120°$, (*e*) $\theta = 160°$, (*f*) $\theta = 180°$. ○, ●, experiment; ——, inviscid theory (from Chow *et al.* 1976).

number R_θ, the shape parameter H_{12} and the wall shear stress coefficient C_f, along the body. The decrease in the shape factor with distance is similar to two-dimensional relaxing flows, but the decrease in C_f is peculiar to this axisymmetric flow. One would have expected a recovery of C_f upwards in a two-dimensional flow. However, the significant flow convergence produced by the body geometry in this range of x/L prevents this trend in the axisymmetric flow. Nevertheless, it is seen from figure 7 that the measured velocity distributions indicate the existence of the universal semi-logarithmic behaviour in the near-wall region and confirm the effectiveness of the trip wire used to fix transition. The velocity distributions shown in this figure are not corrected for probe displacement and shear effects, in view of the uncertainties involved in making such corrections.

3.2. *Measurements at* 15° *incidence*

Figure 8 shows some typical longitudinal distributions of the wall static pressure along several generators from $\theta = 0$ (windward side) to $\theta = 180°$ (leeward side). In each case, the experimental data are compared with the results of the inviscid-flow calculations. It is seen that inviscid-flow theory predicts the wall pressure distribution

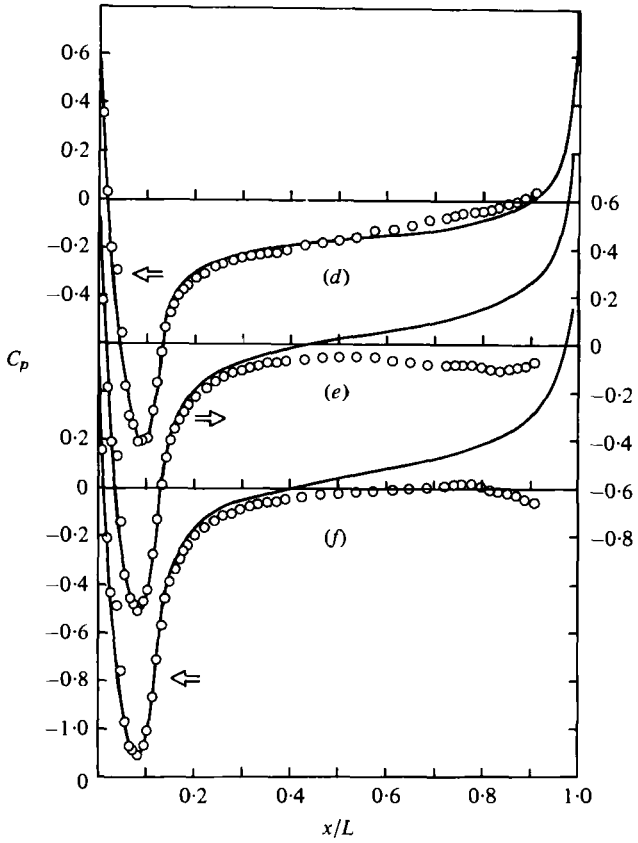

FIGURE 8(*d–f*). For legend see p. 489.

accurately only for $x/L < 0{\cdot}7$ near $\theta = 0$ and $x/L < 0{\cdot}2$ near $\theta = 180°$. The observation that the predicted minimum pressure coefficient is in good agreement with the measurements at all θ positions indicates that the tunnel blockage is still negligible at this angle of attack and that the disagreement between the inviscid and experimental pressure distributions further downstream cannot be attributed to this effect. This disagreement is demonstrated even more dramatically in figure 9, which shows the pressure distribution in the transverse direction at some axial locations. The detailed boundary-layer measurements discussed below show that the differences between the inviscid and measured surface pressure distributions are due to a strong interaction between the boundary layer and the external flow (i.e. viscous–inviscid interaction) associated with massive local thickening of the boundary layer and the formation of an embedded vortical flow.

Before discussing the boundary-layer measurements, it is useful to note some of the important characteristics of the surface pressure distribution. Figure 8 shows that, in the axial direction, the pressure gradient is generally mild after the initially strong favourable and adverse gradients. Thus, in the terminology of two-dimensional flow, the present boundary-layer measurements were made in a region ($0{\cdot}176 \leqslant x/L < 0{\cdot}759$) of relaxing longitudinal pressure gradients. Over the windward side of the body ($0 < \theta < 100°$, say) the viscous interaction results in an accentuation of the adverse

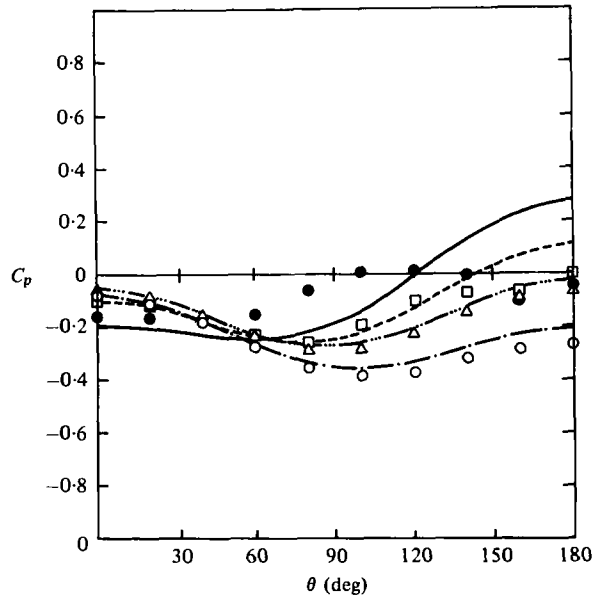

FIGURE 9. Typical circumferential distributions of wall static pressure on the body of revolution at 15° incidence. Individual points represent experimental data and continuous lines represent inviscid theory. Values of x/L are: ○, —·—, 0·176; △, —···—, 0·333; □, - - - -, 0·648; ●, ——, 0·889.

pressure gradient over that predicted by inviscid theory. Thus, the favourable inviscid pressure gradient along $\theta = 0$ to 40° for x/L greater than about 0·7 is relieved, while the mild favourable and adverse inviscid pressure gradients along $\theta = 60°$ for x/L greater than 0·7 are replaced by strong adverse pressure gradients in the real flow. This situation is reversed over the leeward side of the body. For $\theta = 140$–180°, the strong adverse pressure gradients predicted by inviscid-flow theory are relieved to such an extent that along the leeward symmetry plane the boundary layer develops under the influence of a near-zero pressure gradient that becomes favourable further downstream. It is necessary to mention here that the apparent agreement between theory and experiments in the intermediate zone, around $\theta = 120°$ for example, is purely accidental.

An important quantity in the development of a three-dimensional boundary layer is the pressure gradient in the transverse direction since it determines the magnitude and direction of the crossflow. Figure 9 shows the marked differences between the gradients in the real flow and those predicted by inviscid theory. Furthermore, a comparison of the data in figures 8 and 9, taking due account of the body radius, indicates that over most of the body surface the transverse pressure gradients are dominant over the longitudinal gradients. The measured pressure distributions (figure 9) indicate strong adverse transverse pressure gradients in the (approximate) region $90 < \theta < 150°$. One may therefore expect the circumferential flow to reverse, under the influence of this gradient, at least over some part of the region. The velocity profile measurements confirmed such a reversal.

The plane-of-symmetry boundary layer. Owing to the absence of cross-flow, the behaviour of the boundary layer in the plane of symmetry is somewhat simpler to analyse. It is intermediate in complexity between the axisymmetric boundary layer

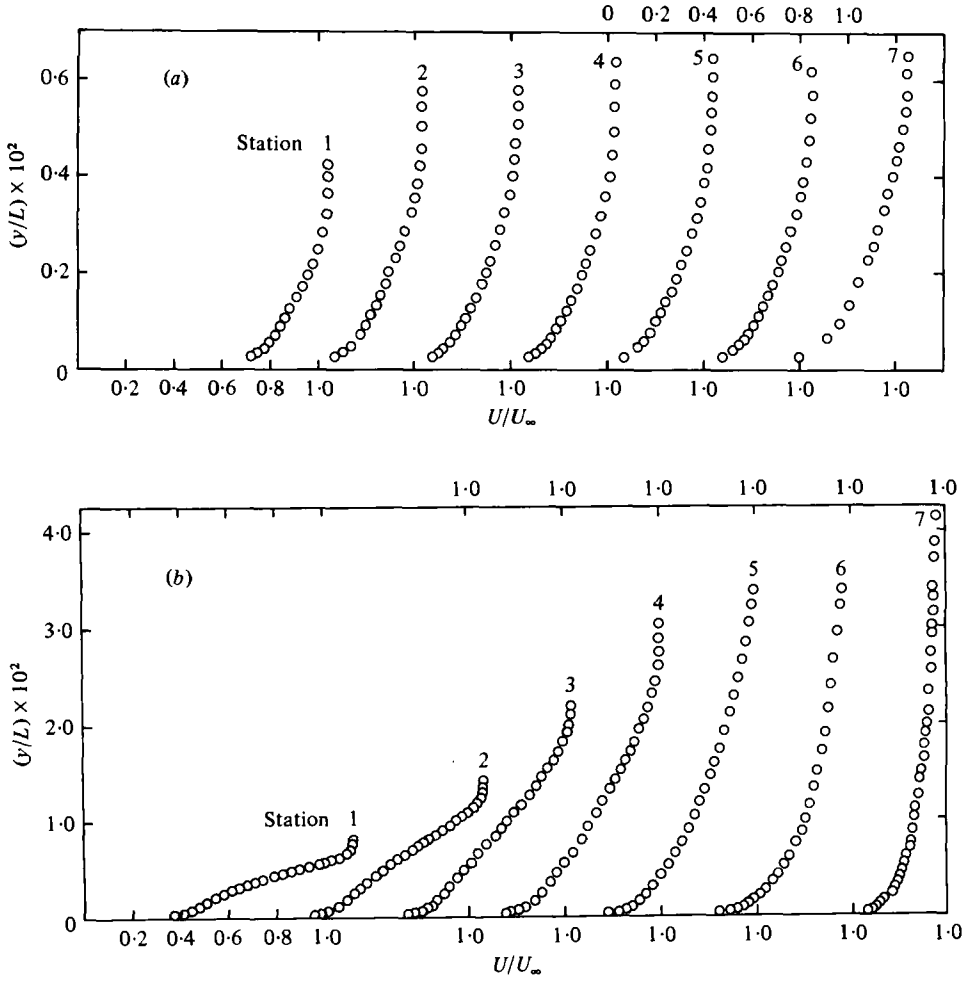

FIGURE 10. Mean velocity distributions in the plane of symmetry boundary layer at $\theta = 15°$, (*a*) windward side ($\theta = 0°$), (*b*) leeward side ($\theta = 180°$).

and the fully three-dimensional boundary layer. Although the cross-flow component of velocity, W, in the circumferential direction, is locally zero, its circumferential gradient, $\partial W/\partial\theta$, is non-zero (even in the irrotational flow outside the boundary layer) and is a measure of the lateral convergence, or divergence, of streamlines into, or out of, the plane of symmetry.

The velocity profiles measured along the windward ($\theta = 0$) and leeward ($\theta = 180°$) sides of the plane of symmetry are shown in figures 10(*a*, *b*), and the corresponding integral parameters (boundary-layer thickness δ, displacement and momentum thicknesses δ_1 and δ_2, shape parameter $H_{12} \equiv \delta_1/\delta_2$ and the wall shear-stress coefficient C_f) are shown in figures 11(*a*, *b*). The velocity profiles were obtained at stations 1 to 7 for the body at 15° incidence. However, since the body was too slender to accommodate the traverse mechanism at station 7 a specially designed extension arm was used for the traverse. Also, at this station the boundary-layer thickness at $\theta = 180°$ as well as in most of the leeward region exceeded the range of the traverse potentiometer.

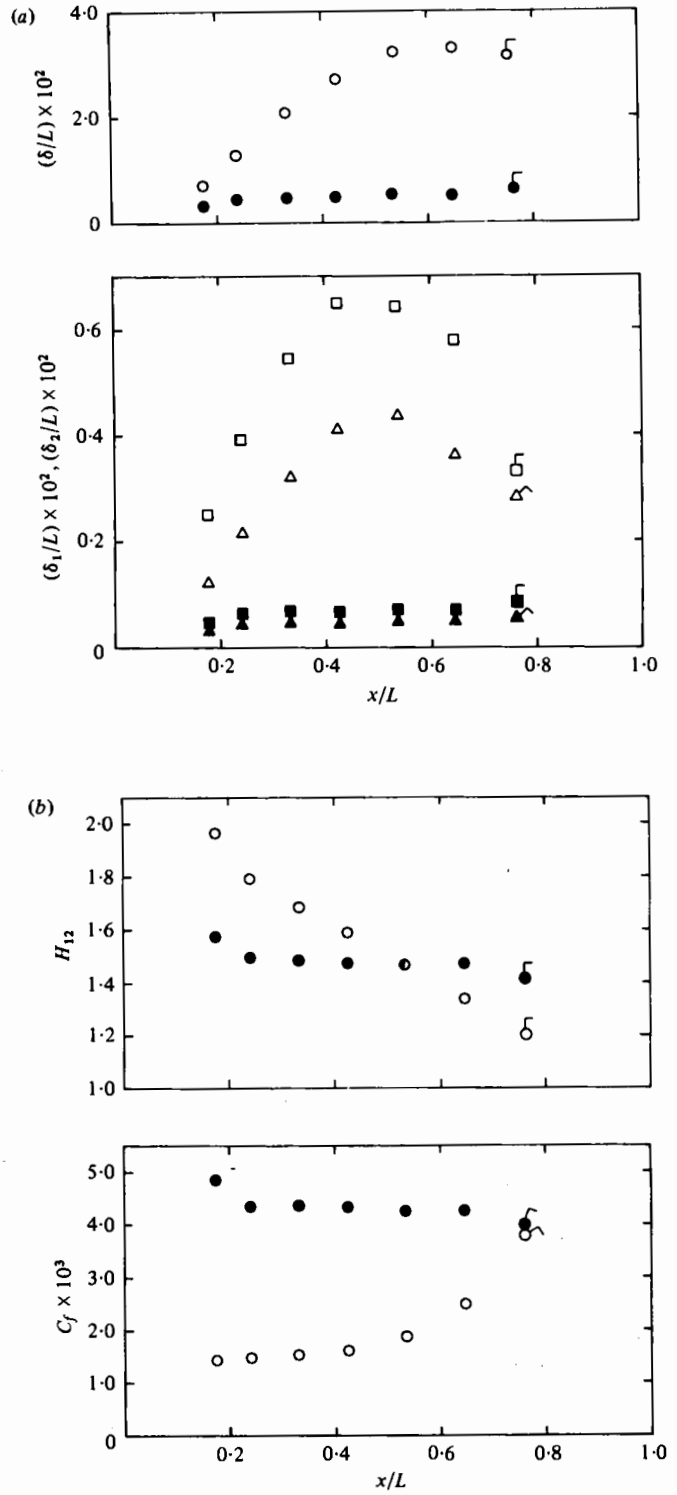

FIGURE 11. Development of the plane of symmetry boundary layers at $\alpha = 15°$. Filled symbols refer to the windward side ($\theta = 0°$) and open symbols refer to the leeward side ($\theta = 180°$). (Note that in (*a*, *b*) and elsewhere, data for station 7 are represented by flagged symbols. This is done in order to remind the reader that data for station 7 are to be interpreted with some caution owing to possible inaccuracies in these measurements.)

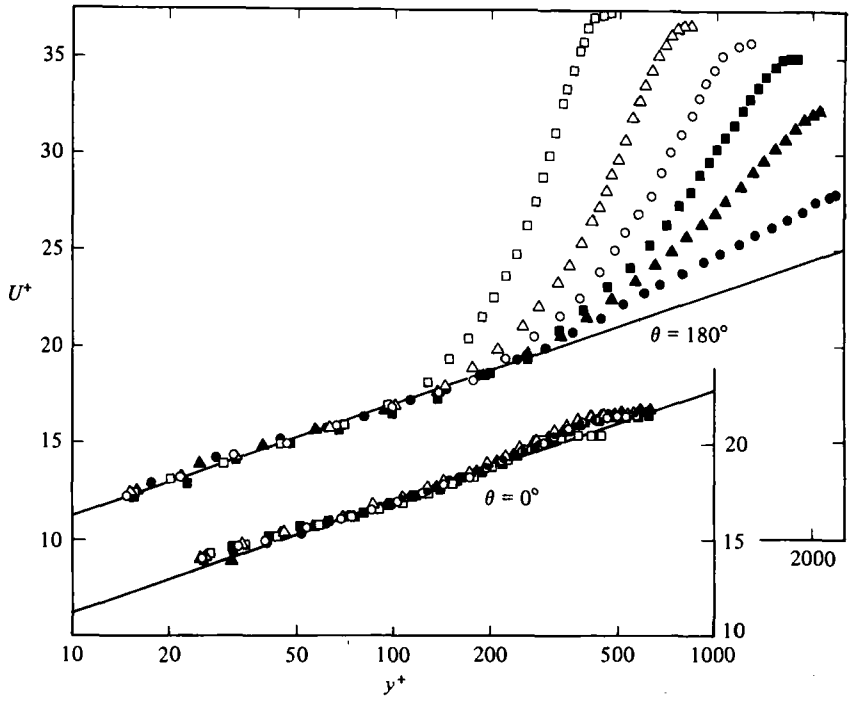

FIGURE 12. Velocity distributions in the plane of symmetry boundary layers at $\alpha = 15°$, in wall-layer co-ordinates. Symbols as in figure 7.

It therefore became necessary to carry out the traverse in two stages. The results from the inner and outer traverses had to be later patched together. Results for station 7 should, wherever presented, therefore be considered somewhat less accurate than those for the first six stations. These results have been, nevertheless, included as they provide a more complete picture of the three-dimensional boundary-layer development over the body.

Before the present experiments were started, there was some doubt as to whether the boundary layer on the windward side could be maintained in a turbulent state in spite of the presence of the trip wire, since earlier experiments by Pavamani (1960) on a triaxial ellipsoid had indicated a trend towards delayed transition in the presence of strong streamline divergence. However, the measurements indicate that the present trip wire was effective in producing a fully turbulent boundary layer even at the first measuring station over the entire circumference. This is well demonstrated by the plane-of-symmetry velocity profiles plotted in wall-layer co-ordinates in figure 12. The universal semilogarithmic distribution exhibited by all the profiles also justifies the use of the Preston tube for the measurement of wall shear stress on the plane of symmetry. It is also interesting to observe that the wake component of the velocity is suppressed along $\theta = 0$ as well as $\theta = 180°$. This is perhaps largely due to the effect of the streamline divergence present everywhere across the boundary layer in the former case and over a significant part of the boundary layer in the latter case. It is, however, difficult to isolate this effect from other effects present in this flow, such as longitudinal pressure gradient and possibly Reynolds-number effects.

In the interpretation of the results shown in figures 10 and 11, it is essential to bear in mind the magnitude and sense of the pressure gradients in the neighbourhood of the plane of symmetry. It is seen that the velocity profiles along the windward side ($\theta = 0$) do not contain inflexion points. This is to be expected in view of the favourable longitudinal pressure gradient (figure 8*a*) prevailing over the region of measurement. The shape of the profile at the most upstream station (station 1) also indicates that the boundary layer has recovered from the effect of the strong adverse pressure gradient further upstream. On the other hand, the velocity profiles on the leeward side ($\theta = 180°$) are characteristic of the adverse longitudinal pressure gradient present along the generator. The boundary layer is seen to recover gradually from the initially strong pressure gradient as the flow progresses downstream.

It is particularly important to note that there is no reversal of the axial velocity (flow 'separation' in a two-dimensional sense) on either side (windward or leeward) of the plane of symmetry over the region covered by the measurements. This confirms the result of a preliminary wool-tuft survey which had indicated no axial 'flow reversal' anywhere on the body. Another important observation to be made is the significant difference in the thickness of the boundary layer on the two sides of the plane of symmetry: the boundary layer on the leeward side is about 6 times thicker than that on the windward side. This is brought about by the circumferential pressure distribution on the body and the cross-flow associated with it, as will be discussed later. Some of the contrasting features of the boundary layer on the two sides are further depicted by the development of the integral parameters shown in figure 11. Along $\theta = 0$, the boundary layer is continuously subjected to a mild favourable pressure gradient after a short fetch of adverse pressure gradient upstream of station 1. The initial, relatively rapid development of the boundary-layer parameters [not very clearly noticeable in figure 11(*a*) owing to the rather small scale, but more readily seen from figure 11(*b*)] due to the delayed effect of the adverse pressure gradient is subsequently slowed down under the combined influence of the favourable pressure gradient and the continued divergence of the streamlines out of the plane of symmetry. The value of C_f remains high over the entire region. Along $\theta = 180°$, on the other hand, the initial adverse pressure gradient and flow convergence cause the boundary layer to grow rapidly and C_f to drop to a low value at station 1. As the adverse pressure gradient is relaxed beyond this station, this effect, together with the subsequent divergence of streamlines out of the plane of symmetry (beginning around $x/L = 0{\cdot}25$, as shown in figure 16) associated with reversal of the circumferential component of velocity elsewhere on the body (see, for example, Han & Patel 1979), arrests the expected decrease in C_f. In fact, the strong influence of streamline divergence eventually causes the skin-friction coefficient to *increase* and the shape factor to *decrease* even though the boundary-layer thicknesses δ, δ_1 and δ_2 continue to grow. Ultimately, however, the influence of streamline divergence becomes strong enough not only to arrest the increase but actually to cause a reduction in the various thicknesses.

The boundary layer not in the plane of symmetry. Yaw-probe traverses were made along the five generators $\theta = 30$, 60, 90, 120 and 150°. The distributions of Q and γ were obtained at 7 longitudinal stations along each generator. Additional measurements were made along $\theta = 165°$ at a few downstream stations where both Q and γ were found to change dramatically across the boundary layer. It should be noted that

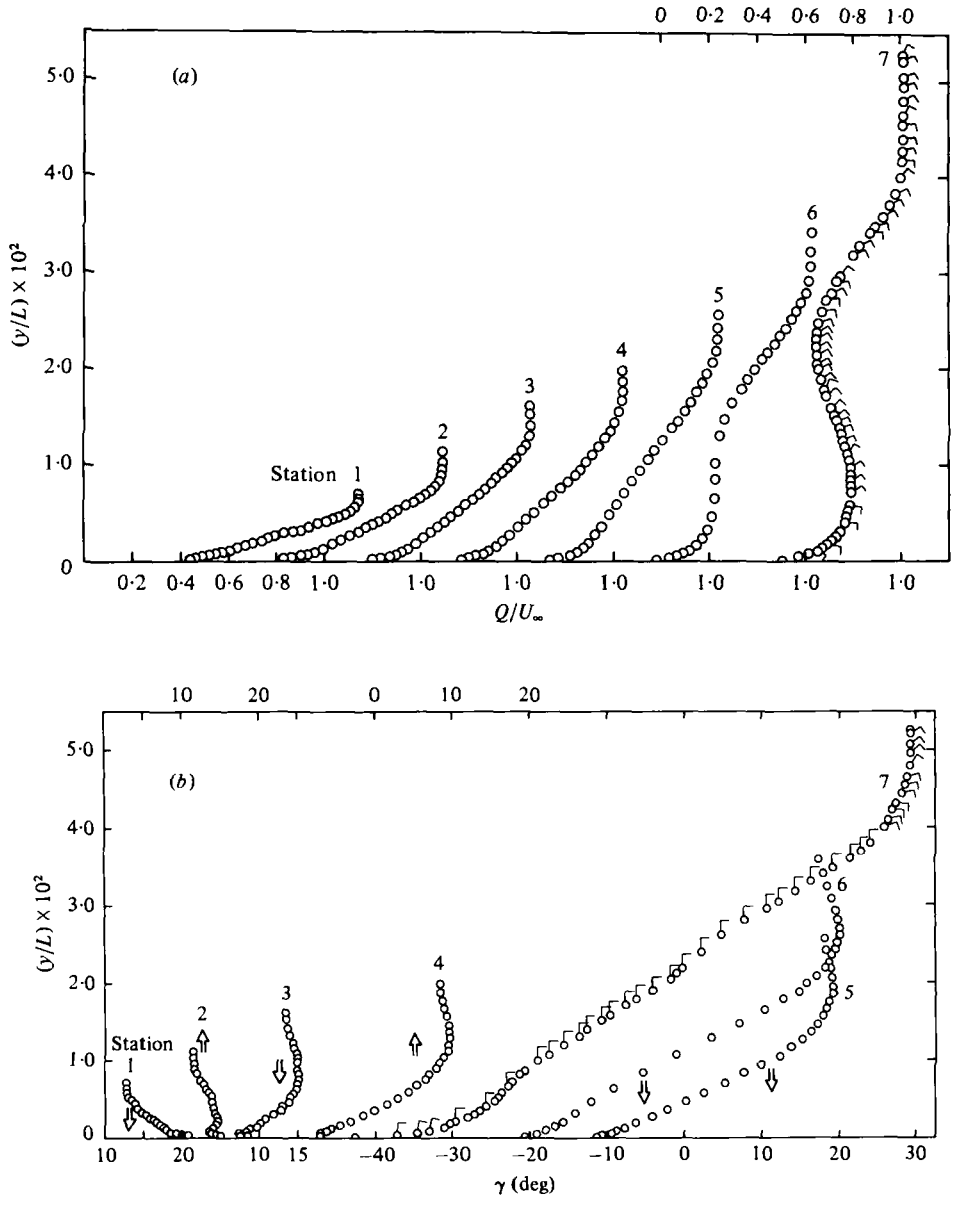

FIGURE 13. Typical distributions of the magnitude Q and the direction γ of the velocity vector $\mathbf{Q}$ in the offplane of symmetry boundary layers at $\alpha = 15°$. $\theta = 150°$. (*a*) Q, (*b*) γ.

γ is the angle between the velocity vector and the local generator of the body. The 'cross-flow angle', usually defined as the angle between the velocity vectors within and outside the boundary layer, and denoted by β, is then $(\gamma - \gamma_e)$, where the subscript e refers to the edge of the boundary layer.

Typical distributions of Q and γ across the boundary layer are illustrated in figure 13 for the $\theta = 150°$ generator. The rapid growth of the boundary layer and the large changes in the direction of the velocity vector within the boundary layer are apparent

from this figure. It is seen that at station 1, the cross-flow angle at the wall is of the order of 10° and across the entire boundary layer the cross-flow velocity is directed towards the leeside of the external streamline. Also, the angle between the velocity vector and the generator varies from 10° at the edge of the boundary layer to more than 20° near the surface. These angles change rapidly in the downstream direction. The cross-flow reverses sign within the boundary layer between stations 2 and 3, giving rise to the so-called cross-over or S-shaped cross-flow profiles. Eventually, at the most downstream station 7 the cross-flow is directed almost entirely towards the windward side of the external streamline and the wall cross-flow angle is of the order of 70–75°. The circumferential component of velocity itself changes sign near the wall between stations 3 and 4, so that, at station 4, for example, the velocity vector is directed towards the windward side of the generator in the inner one-third of the boundary layer and towards the leeward side over the outer two-thirds. The rather peculiar shapes of the total velocity profiles at stations 6 and 7 (see figure 13*a*) are obviously associated with the large changes in the direction of the velocity vector across the boundary layer at these stations. Such shapes have also been observed in boundary layers over ship sterns (see, for example, Larsson 1974; Hoffmann 1976; Hatano, Mori & Hotta 1978) where the flow is also characterized by large changes in streamline direction.

The measurements of Q and γ along other generators demonstrated features similar to those depicted in figure 13 to varying degrees. Over a large region on the windward side, $\theta \leqslant 90°$ say, the total velocity profiles were found to be similar in shape to those shown in figure 10(*a*) for $\theta = 0°$; the cross-flow was unidirectional, i.e. towards the leeside of the external streamlines, and the near-wall cross-flow angles were of the order of 10°. Velocity profiles containing inflexion points, resembling those at stations 2–5 in figure 13(*a*), began to appear at the most downstream stations along $\theta = 120°$, and at more upstream locations for larger θ. These were accompanied by changes in the velocity-vector directions similar to those noted above for $\theta = 150°$.

It should be noted that the values of Q and γ were obtained using the yaw-probe calibrated in a relatively uniform, shear-free flow. These values have not been corrected for other probe-displacement or shear effects since appropriate correction procedures are not known at the present time. It is therefore possible that the first few measurements near the wall, particularly in the region where the boundary layer is thin, may be subject to these errors. Further, as already mentioned, the value of γ_w could not be measured accurately using the equivalent Preston tube method and hence is not shown as a data point in figure 13(*a*). An approximate value of γ_w can perhaps be obtained, as is often done, by extrapolating the measured γ distribution up to the wall, but this may be in substantial error due to the rapid skewing of the flow in the sublayer and the blending zone (depending upon the relative magnitudes of the pressure gradients in the two orthogonal directions (see, for example, Nash & Patel 1972), and the fact that pitot-tube data usually do not penetrate sufficiently into these regions.

The overall growth of the three-dimensional boundary layer over the body is illustrated in figure 14 by means of three-dimensional plots of the wall shear-stress coefficient

$$C_f = \tau_w / \tfrac{1}{2}\rho Q_e^2$$

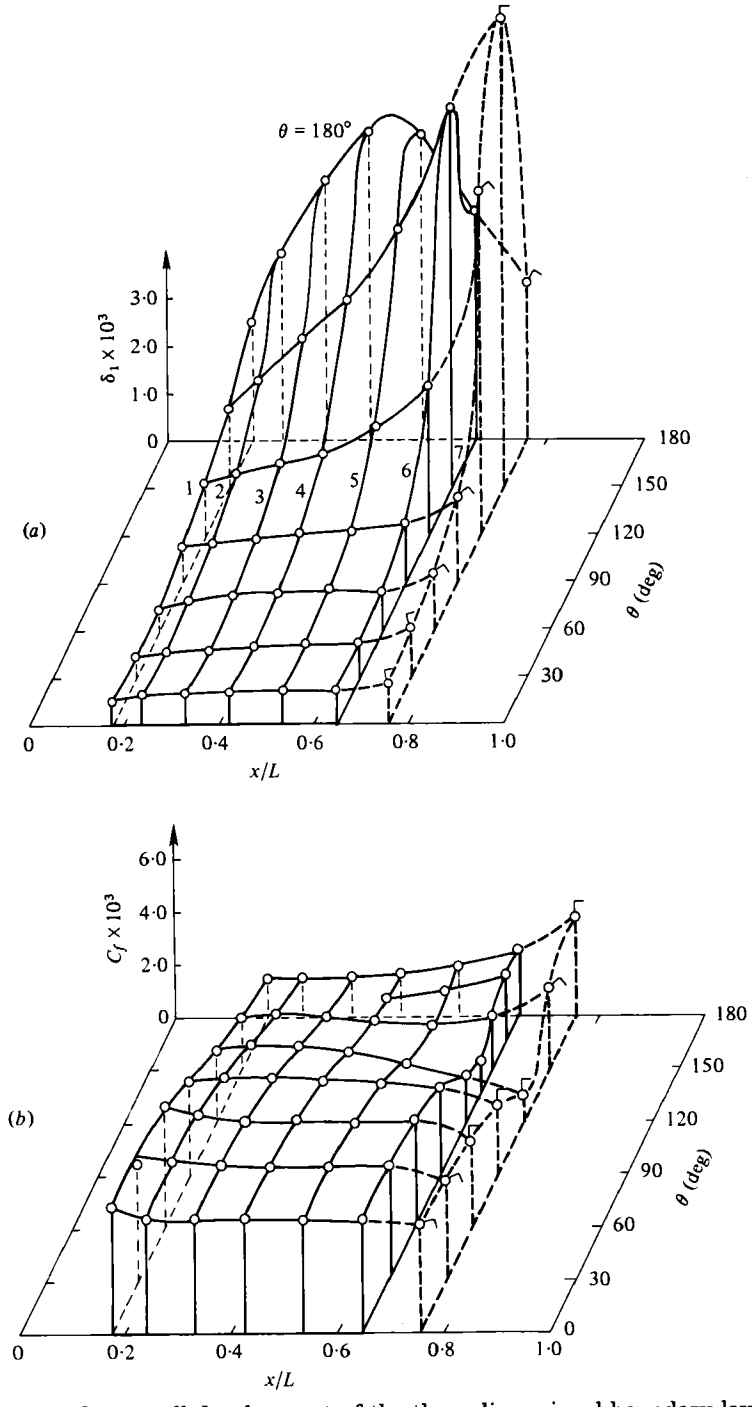

FIGURE 14. The overall development of the three-dimensional boundary layer on the body of revolution at 15° incidence. (*a*) δ_1. (*b*) C_f.

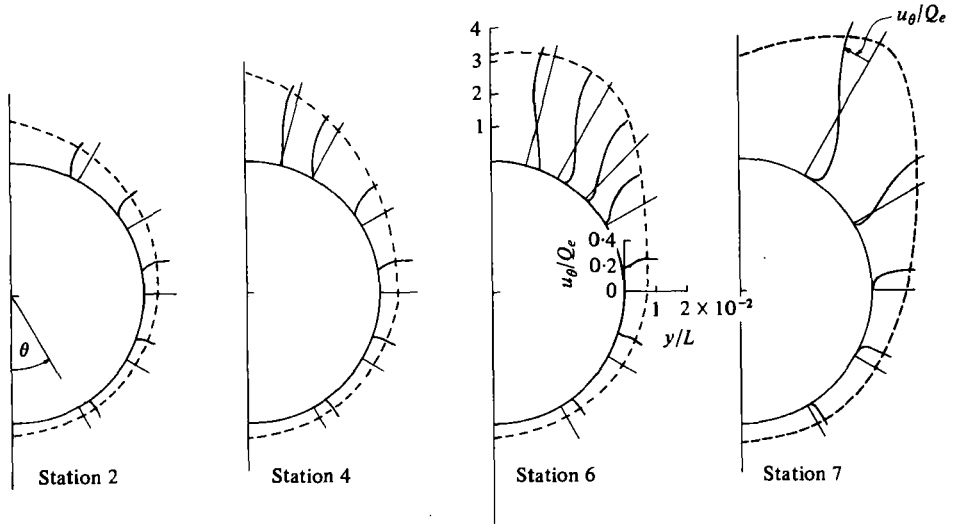

FIGURE 15. The distributions of the circumferential component of the velocity across the boundary layer. The dotted line denotes the edge of the boundary layer (based on 99·5 per cent of Q_e). Scales are the same for all the stations as shown for station 6.

and a representative 'displacement' integral

$$\delta_1 = \frac{1}{Q_e}\int_0^\delta (U_e - U)\,dy.$$

It should be noted that δ_1 is associated only with the axial component of velocity and is not the true displacement thickness of the boundary layer. Nevertheless, it can be used as a measure of the boundary-layer thickness. Figure 14 shows the rapid growth of the boundary layer over the leeward side of the body. In particular, it is observed that the maximum boundary-layer thickness occurs in the neighbourhood of the $\theta = 150°$ generator. The decrease in thickness beyond $x/L \cong 0{\cdot}5$ along $\theta = 180°$ is associated with severe flow divergence in the inner part of the boundary layer along the leeward plane of symmetry. The distribution of C_f is not as spectacular as that of δ_1, but it clearly indicates the absence of any singular separation ($C_f = 0$) over the region of measurement. The characteristic decrease in C_f at stations 6 and 7 in the region of $\theta = 120°$ is of special significance since it indicates that a singular separation point ($C_f = 0$) may be imminent with further increase in incidence. The occurrence of such a singularity ahead of flow reversal on either side of the plane of symmetry has been observed in the recent laminar boundary-layer calculations of Patel & Choi (1979) and Cebeci, Khattab & Stewartson (1979) on a spheroid at incidence.

The circumferential development of the boundary layer is illustrated very vividly in figure 15. Up to station 4, the circumferential component of velocity is unidirectional and therefore the resultant velocity vectors are skewed from the windward to the leeward side. This monotonic convergence of streamlines towards the leeward side leads to the continuous thickening of the boundary layer in the circumferential direction, with the maximum thickness occurring on the leeward plane of symmetry as seen from figure 14(*a*). Further downstream, the circumferential flow reverses direction in the inner part of the boundary layer in the neighbourhood of the leeward

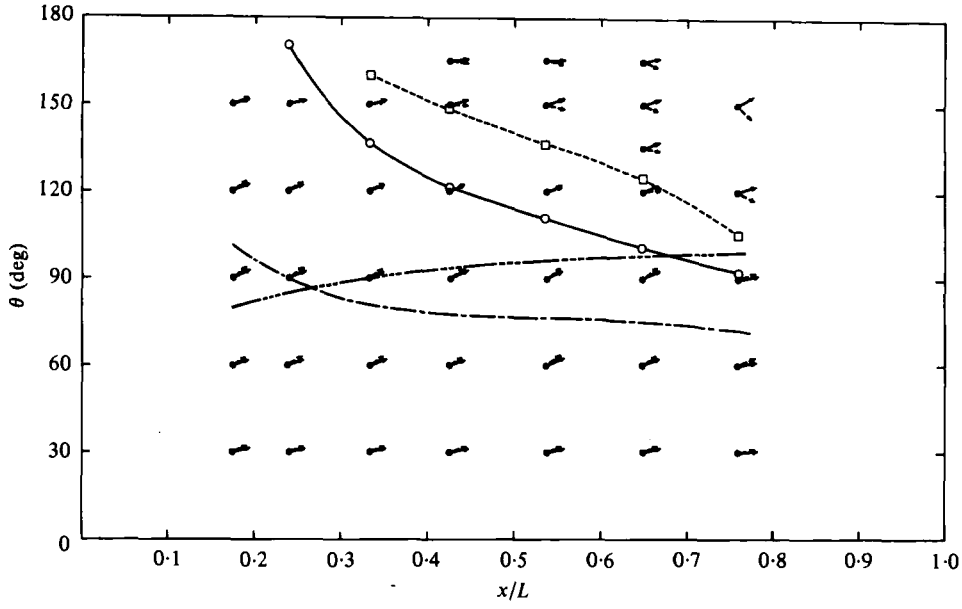

FIGURE 16. Some important features of the three-dimensional flow over the body of revolution at 15° incidence. →, orientation of freestream velocity vector; –→, orientation (approximate) of the limiting velocity vector at the wall; ——, line of cross-flow reversal; – – –, line of circumferential flow reversal; — · —, locus of minima of circumferential pressure distribution (measured); — · · · —, locus of minima of circumferential pressure distribution (from inviscid theory).

symmetry plane but continues to be directed from the windward to the leeward side in the outer part of the boundary layer. This reversal occurs at $\theta \cong 137$, 124 and 105° at stations 5, 6 and 7, respectively. The movement of the circumferential-flow reversal point away from the leeward side is also accompanied by a shift in the location of the maximum boundary-layer thickness and is correlated with the peak in δ_1 and the valley in the magnitude of the wall shear stress distributions shown in figures 14 (a, b). Figure 15 also shows very clearly the development of a vortical structure within the boundary layer. Thus, the flow over some circumferential extent from the leeward side of symmetry plane may be viewed as a longitudinal vortex embedded inside a thickening boundary layer. The vortex appears to grow in 'size' and its 'centre' appears to move further and further away from the surface and the leeward plane of symmetry as the flow progresses downstream. It is essential to emphasize, however, that the measurements do not indicate any catastrophic change in the flow properties, the changes in the velocity profiles being smooth and gradual. Nevertheless, the first impression conveyed by the results, especially in view of the pressure distribution and viscous–inviscid interaction discussed earlier, is that the flow can no longer be treated within the framework of thin boundary-layer theory.

Figure 16 depicts effectively several additional important features of the three-dimensional flow. It shows a map of the orientation γ_e of the measured freestream velocity vectors and the orientation γ_{wa} of the measured near-wall velocity vectors. The latter is not the actual direction of the wall streamline or the wall shear-stress since, as noted earlier, this could not be measured accurately with the yaw probe.

γ_{wa} is simply the flow angle indicated by the yaw probe (using the external flow calibration) when it is just touching the surface. Thus, at best, it is the direction of the flow at a distance one-half of the probe height (0·4 mm) from the surface. From these mappings, one can obtain two important lines, namely the line of reversal of the cross-flow near the wall, given by $\gamma_{wa} = \gamma_e$, and the line of reversal of the circumferential component of velocity, given by $\gamma_{wa} = 0$. It is seen that these lines appear to originate from the leeward plane of symmetry in the neighbourhood of $x/L = 0{\cdot}25$. As will be discussed later, these lines assume special significance in the development of boundary-layer calculation methods. Also shown in figure 16 are the loci of minima of the circumferential pressure distributions shown typically in figure 9. One of these loci corresponds to the inviscid-flow pressure distribution and the other corresponds to the measured pressure distribution. The marked difference between the two indicates the global effect of the viscous–inviscid flow interaction on the body.

4. Discussion and conclusions

The experimental results presented here clearly demonstrate the complexities of the three-dimensional boundary layer on a body of revolution at incidence. The present experiment differs from previous investigations insofar as it provides quantitative information on some of the extreme features of a three-dimensional turbulent boundary layer. For example, here we have the case of a boundary layer whose growth in the transverse direction is more spectacular than in the longitudinal, primary direction. In spite of the zero-cross-flow constraint imposed by the plane of symmetry, the boundary layer accommodates large and reversing cross-flows over a significant portion of the body. Other, intricately related features include the development of a vortical structure within the boundary layer, and the presence of a large region of strong viscous–inviscid flow interaction in spite of the absence of any catastrophic breakaway (separation) of the viscous flow from the surface. To be sure, many of these phenomena have been observed in previous experimental studies (largely through flow visualizations on aircraft and missile configurations) and some have been predicted by numerical solutions restricted to laminar flow. However, the data presented here document these quantitatively in some detail and for the first time. Hence, these data would prove valuable not only in the general understanding of three-dimensional turbulent boundary layers but also in guiding the development of appropriate methods of prediction of such flows.

In a series of papers, Wang (1970, 1972, 1974*a–c*, 1975) has presented the results of numerical solutions of the laminar boundary layer on a 4:1 spheroid at several incidences. Although the present experiment is concerned with turbulent flow and a quite different geometry, the data qualitatively confirm some aspects of his results. These include the differences between the flows on the leeward and windward sides of the plane of symmetry as well as the reversal of the circumferential component of velocity or wall shear stress along a well-defined line on the body.

One of the primary objectives of the present experiment was to study the characteristics of the boundary layer in the neighbourhood of what Wang (1972, 1974*a*) has termed an open separation. An open separation line is akin to the free-vortex separation line of Maskell (1955). According to Wang, such a separation line does not cross the plane of symmetry of the body. The flow on either side of it is fed entirely from

upstream and it is recognized by streamlines coming together from either side of it and leaving the surface along it to form a longitudinal vortex. Wang further suggested that, although such a separation line runs closely to the locus of points of zero circumferential component of wall shear stress, the two lines do not, in general, coincide. This graphic description of an open separation line is supported only by conceptual sketches made by Wang on the basis of his calculations, which, for large angles of attack, could be carried out only in the region between the windward symmetry plane and the line of circumferential-flow reversal, and previous visual studies. The results of the recent flow visualization investigation conducted by Han & Patel (1979) on a 4·3:1 spheroid at various incidences confirm Wang's model in that the dye patterns on the surface clearly indicate a well-defined line along which surface streamlines from the windward and leeward sides merge and roll up into a vortex further downstream. Although such a line is absent at incidences of the order of 5°, it appears near the tail as the incidence is increased, and moves upstream and becomes longer with further increase in incidence.

It was speculated that, in spite of the fact that the present flow is turbulent and the body geometry is different, the data would indicate the quantitative features of the flow that lead to the formation of an open separation line. This speculation, indeed, turned out to be correct as indicated by an examination of the various views of the data presented here. These data show the beginning of a vortex structure but do not indicate, at least in the region covered by the measurements, any breakaway of the vortex from the surface, as implied by the open separation concept. In fact the absence of a catastrophic breakaway of the vortex allowed the measurements to be made easily and accurately. Although direct measurements of vorticity and the normal component of velocity were not made, the measured distributions of the circumferential component of velocity (figure 15) indicate a progressive strengthening of the longitudinal component of vorticity in the downstream direction. This component of vorticity becomes a maximum somewhere between the line of circumferential flow reversal shown in figure 16 and the leeward generator, and would tend to rotate the resultant vorticity vector into the longitudinal direction. The occurrence of a longitudinal vortex and its eventual breakaway from the surface, in the manner implied by the concept of open separation, would presumably depend upon the strength and concentration of the longitudinal component of vorticity relative to the circumferential component. Nevertheless, the development of the longitudinal component of increasing strength can be viewed as a vortical structure embedded in the boundary layer, and provides the mechanism for the generation of a distinct vortex.

Apart from providing some insight into the origin of the vortex structure, the present data will be useful in the development of calculation methods that are concerned with the prediction of three-dimensional turbulent boundary layers not only on bodies of revolution at incidence but also on related configurations such as finite wings, aircraft fuselages, and ship hulls. A review of such methods would not be appropriate here, but it is useful to consider, in view of the present experimental results, certain general features that require careful treatment. Among these are the following. (i) The rapid changes in the properties of the boundary layer in the circumferential direction, even before the onset of circumferential flow reversal or open separation, indicates that their description would require calculation procedures that are at least as accurate in the transverse direction as in the longitudinal direction.

The present data, therefore, provide a crucial test case for the examination of the relative merits of different numerical methods. (ii) In the event of circumferential flow reversal, the proper demarcation of the zones of dependence and influence is of paramount importance since the velocity profiles at points in the neighbourhood of such reversals are determined by a large upstream zone of influence. For example, it is seen from figure 16 that a calculation method that marches in the circumferential direction starting from either the windward or the leeward side of the plane of symmetry can proceed only up to the line of circumferential flow reversal. The present data can be used to verify the performance of the few calculation methods which claim to address such flow reversals. (iii) The gradual evolution of an open separation, on the one hand, and the lack of any singular behaviour in the usual thin boundary-layer equations, on the other, imply that great care would be needed in the interpretation of results of calculations performed with thin boundary-layer approximations since the calculations may not indicate a catastrophic failure although the underlying assumptions become physically unrealistic. This aspect assumes special importance in the region between the leeward symmetry plane and the line of cross-flow reversal shown in figure 16. (iv) The data also provide an opportunity to evaluate critically some of the recent methods which attempt to predict the surface pressure distribution by matching the viscous and inviscid flows. Within the framework of the displacement thickness concept, the external flow sees a body that is distorted markedly in the neighbourhood of the line of circumferential flow reversal but, as indicated by the measured surface pressure distributions, the influence of the viscous–inviscid interaction is global. In fact, from figures 9 and 16, it is seen that the interactive domain extends approximately over the entire region leeward of the line of measured minimum pressure in figure 16. It is obvious that a successful calculation procedure should correctly account for this large and global viscous–inviscid interaction. (v) Finally, one of the aims of a boundary-layer calculation, or its extension, should be to predict the location of any closed or singular separation on the body, as depicted in the flow-visualization experiments of Han & Patel (1979). Such a separation was not observed in the present experiments. However, the possibility that the boundary-layer approximations break down (as suggested by the present data) in the region of open separation, which, when present, usually occurs upstream of a singular separation, needs to be explored by comparison of calculations with experimental data. A successful downstream-marching solution for the flow on either side of an open separation line may require the incorporation of additional terms in the boundary-layer equations and allowance for viscous–inviscid interaction.

This research was supported in part by Grant no. DAAG29-76-G-0036 from the U.S. Army Research Office. Partial support was also provided by the Lockheed-Georgia Company in the later stages of the study. The authors are grateful to Mr T. Han for his assistance with the preliminary measurements.

REFERENCES

Cebeci, T., Khattab, A. A. & Stewartson, K. 1979 Prediction of three-dimensional laminar and turbulent boundary layers on bodies of revolution at high angles of attack. *Proc. 2nd Sym. on Turbulent Shear Flows, Imperial College*, pp. 15.8–15.13.

CHOW, S. K., HOU, A. Y. & LANDWEBER, L. 1976 Hydrodynamic forces and moments acting on a body emerging from an infinite plane. *Phys. Fluids* **19**, 1439–1449.

HAN, T. & PATEL, V. C. 1977 Flow-visualization of three-dimensional boundary-layer separation on bodies of revolution at incidence. *Univ. Iowa, Iowa Inst. Hydraulic Res. Rep.* no. 205.

HAN, T. & PATEL, V. C. 1979 Flow separation on a spheroid at incidence. *J. Fluid Mech.* **92**, 643–657.

HATANO, S., MORI, K. & HOTTA, T. 1978 Experimental and theoretical investigations of ship boundary layer and wake. *Proc. 12th Symp. on Naval Hydrodynamics, Washington, D.C.*

HOFFMANN, H. P. 1976 Untersuchung der 3-dimensionalen, turbulenten Grenzschicht an einem Schiffsdoppelmodell im Windkanal. *Univ. Hamburg, Inst. für Schiffbau, Rep.* no. 343.

JOHNSTON, J. P. 1976 Experimental studies in three-dimensional turbulent boundary layers. *Reviews in Viscous Flow, Proc. Lockheed-Georgia Symposium, Atlanta*, pp. 239–290.

LANDWEBER, L. & MACAGNO, M. 1969 Irrotational flow about ship forms. *Univ. Iowa, Iowa Inst. Hydraulic Res., Rep.* no. 123.

LARSSON, L. 1974 Boundary layers of ships. III. An experimental investigation of the turbulent boundary layer on a ship model. *Swedish State Shipbldg Expt. Tank, Rep.* no. 46.

MASKELL, E. C. 1955 Flow separation in three dimensions. *British Aero. Res. Counc., Rep.* no. 18060.

NASH, J. F. & PATEL, V. C. 1972 *Three Dimensional Turbulent Boundary Layers.* Atlanta: SBC Tech. Books.

PATEL, V. C. 1965 Calibration of the Preston tube and limitations on its use in pressure gradients. *J. Fluid Mech.* **23**, 185–208.

PATEL, V. C. & CHOI, D. H. 1979 Calculation of three-dimensional laminar and turbulent boundary layers on bodies of revolution at incidence. *Proc. 2nd Symp. on Turbulent Shear Flows, Imperial College*, pp. 15.14–15.24. (To be published in *Turbulent Shear Flows* II, Springer, 1980.)

PAVAMANI, F. S. A. 1960 Three dimensional turbulent boundary layer. M.S. thesis, Mech. Hydr. Program, University of Iowa.

RAJARATNAM, N. & MURALIDHAR, D. 1968 Yaw probe used as a Preston tube. *Aero J., Roy. Aero. Soc.* **72**, 1059–60.

RAMAPRIAN, B. R., PATEL, V. C. & CHOI, D. H. 1978 Mean flow measurements in the three-dimensional boundary layer over a body of revolution at incidence. *Univ. Iowa, Iowa Inst. Hydraulic Res., Limited Distribution Rep.* 56.

WANG, K. C. 1970 Three-dimensional boundary layer near the plane of symmetry of a spheroid at incidence. *J. Fluid Mech.* **43**, 187–209.

WANG, K. C. 1972 Separation patterns of boundary layer over an inclined body of revolution. *A.I.A.A. J.* **10**, 1044–1050.

WANG, K. C. 1974*a* Laminar boundary layer near the symmetry plane of a prolate spheroid. *A.I.A.A. J.* **12**, 949–958.

WANG, K. C. 1974*b* Boundary layer over a blunt body at high incidence with an open type of separation. *Proc. Roy. Soc.* A **340**, 33–55.

WANG, K. C. 1974*c* Boundary layer over a blunt body at extremely high incidence. *Phys. Fluids* **17**, 1381–1385.

WANG, K. C. 1975 Boundary layer over a blunt body at low incidence with circumferential reversed flow. *J. Fluid Mech.* **72**, 49–65.